Research on Chemical Intermediates (2023) 49:1855–1878
https://doi.org/10.1007/s11164-023-04988-7

Computational analysis of the structural, optoelectronic and photovoltaic properties of triphenylamine-based dyes and their interaction with TiO_2 / Iodine

Malak Lazrak[1] · Hamid Toufik[1] · Sliman Ennehary[1] · Si Mohamed Bouzzine[1,2] · Fatima Lamchouri[1]

Received: 6 November 2022 / Accepted: 18 February 2023 / Published online: 28 February 2023

Abstract

In this work, six molecules M1-M6, with the donor—π-spacer—acceptor structure, based on triphenylamine have been purposely studied to be applied in π-type dye-sensitized solar cells (DSSCs). We explore the effect of different electron-withdrawing substituents on the optoelectronic, structural, and photovoltaic dye properties. The key parameters of all the dyes affecting the power conversion efficiency (PCE) were theoretically investigated in detail using density functional theory (DFT) and TD-BHandHLYP calculations to reveal structure–property relationships. The calculated results show that the strong electron-withdrawing groups of thienothiadiazole and furano-thiadiazole, reduce energy gaps and provide a red shift of absorption spectra. The dye M1 and M3 have presented interesting optoelectronic properties with interesting charge transfer properties. Meanwhile, the enhanced free energy of charge injection (ΔG^{inject}) and light-harvesting efficiency of the M5 dye revealed that this dye can be used as a potential sensitizer for TiO_2-based DSSCs. The DFT method is also used to evaluate the bond interactions between the dye and iodine. The results suggest that dyes containing thienothiadiazole and furano-thiadiazole as π-spacers show more stable interactions with iodine species, thereby increasing the concentration of the redox couple at the surface of the semiconductor. In addition, the process of charge transfer and dye adsorption on $(TiO_2)_9$ cluster was investigated. Calculations show that the M3 dye has lower adsorption energy than the corresponding M1 dye. These results suggest that the adsorption of M3 on the TiO_2 semiconductor would be more stable. The results indicate that the selected dyes provide promising results and motivate future investigations on these new systems.

Keywords Dye-sensitized solar cells (DSSCs) · Triphenylamine · π-bridge · Density functional theory (DFT)

✉ Hamid Toufik
hamid.toufik@usmba.ac.ma

Extended author information available on the last page of the article

Introduction

Solar energy has the advantage of being inexhaustible and of emitting no greenhouse gases when producing electricity. It then constitutes an ecological and economical alternative to fossil fuels which are in limited quantity and whose use is detrimental to the sustainability of organisms [1, 2]. However, the challenge of photovoltaics is to significantly reduce the cost of the energy produced. Silicon currently offers the best performance, but its purification and its treatment lead to very high costs and to an expensive manufacturing process. On the other hand, dye-sensitized solar cells (DSSCs) have attracted considerable attention since the first nanocrystalline solar cell based on a Ruthenium dye developed by Grätzel & *al*, in 1991 [3].

In this type of cell, the dye is responsible, after absorption of a photon, for the generation and the separation of the electron–hole pair by injecting an electron directly into the conduction band of the semiconductor oxide on which it is grafted. The original state of the dye molecule is regenerated by a redox couple system, which itself is regenerated at the counter electrode by electrons passing through the load.

The choice of the different constituents of such a cell is therefore crucial to guarantee the good performance of the device. The dye must meet a certain number of criteria (energy levels, light absorption range, chemical stability, etc.) Based on these requirements, a multitude of dyes, including porphyrins [4–9] and phthalocyanines have been synthesized and tested as light-harvesting components for DSSCs over the past two decades on account of their intense absorption in the visible region of the solar spectrum [10]. However, the dyes based on ruthenium complexes were the first to achieve conversion efficiencies greater than 10% [11–13]. Moreover, as chromophores associated with titanium dioxide and the redox mediator I^-/I_3^-, they have long remained unequaled in terms of performance. Currently, the development of metal-free organic dyes has been of increasing interest over the years because of their low costs and more durable alternatives to ruthenium polypyridyl complexes [14–16]. In addition, they offer greater freedom in terms of molecular engineering [17–19]. The first organic dyes tested, such as perylene [20–22] and coumarin [23–28], had a relatively symmetrical structure and provided only modest energy conversion efficiencies. A breakthrough in the field was instead carried out with organic chromophores "push–pull" of the donor-π-spacer-acceptor type (D-π-A), having a spacer with extended π-delocalized structure. This architecture, which has been the subject of several articles in recent years, has the absorption in the visible range and ensures excellent charge separation at the excited state [29], thus promoting the injection of electrons to the semiconductor while minimizing recombination. The properties of dyes D-π-A can be adjusted by varying the electron donor groups, π-conjugated systems or acceptor units. The D-π-A organic dyes of diverse structures containing electron-donating groups, such as triphenylamine derivatives [30, 31], carbazole [32–34], indole [35, 36] and indoline [37–39] have been developed and resulting in reports of DSSCs with remarkable efficiency. Among

them, triphenylamine-based organic dyes showed higher efficiency compared to those of different structures. The choice of the triphenylamine donor unit in DSSCs is due to their prominent electron donation, greater structural stability and hole-transport ability [40]. Cyanoacrylic acid is most commonly used as an electron acceptor moiety due to the presence of the cyanide and carboxyl groups, which have a strong electron-with drawing capability and strong binding ability to the TiO_2 surface for electron injection [41].

The π-spacer is used to link the electron donor and acceptor, which helps to spread the electron density and facilitate charge separation upon excitation. It plays a significant role in broadening the maximum absorption peak, reducing the charge recombination [42] and efficiently enhance the absorption ability, which is beneficial to improve charge transfer characteristics of DSSCs and increase efficiency [43]. Therefore, choosing the suitable π-spacer is one of the strategies to improve the photovoltaic performances. Several molecules based on heteroaromatic molecules and their derivatives, such as thiophene [44–48], phenyl [49], furan [44, 50–53] and oligothiophene [54, 55], have been explored as π-conjugated systems.

Due to the evolution of computing resources, the exploitation of theoretical methods in the context of computational modeling has experienced considerable growth in the literature. Computational chemistry has been successful in complementing and explaining synthetic results and providing rigorous information where this is inaccessible by experiment [12]. This work takes place in this context. The objective is to develop organic dyes with interesting geometric and optoelectronic properties for photovoltaic applications. The most used method of structural modification, for tuning the highest occupied molecular orbital (HOMO) and the lowest unoccupied molecular orbital (LUMO) energy levels of sensitizer dyes, is by varying the π-conjugated spacer, which is the main objective of this study. We report the characterization of six novel triphenylamine-based push–pull dyes that have been purposely identified to be applied in π-type dye-sensitized solar cells (DSSCs), by using the same electron donor moiety (the triphenylamine group) and the cyanoacrylic acid group as acceptor fragment.

This work aims to demonstrate how the variation of the bridges affects the optoelectronic and electrochemical properties of these dyes. For this purpose, we used different π-conjugated bridges based on the thiadiazole and pyrazine derivatives, such as thienothiadiazole (TT), pyrrolo-thiadiazole (PT), furano-thiadiazole (FT), thienopyrazine (TP), pyrrolo-pyrazine (PP), furano-pyrazine (FP) (Fig. 1).

Another important aspect of DSSCs is the interaction between the dye sensitizer and the TiO_2. The sensitizer molecules have usually a carboxyl group that interacts with the solid electrode. It is of fundamental importance the determination of the geometric structure of the adsorbed dye state and the electronic coupling with the TiO_2 conduction band.

Moreover, other factor, which must be considered when designing organic molecules for DSSCs, is that the dye should be able to prevent charge recombination processes. For most DSSCs, an iodide/triiodide (I^-/I_3^-) redox couple is employed as its electrolyte. Therefore, we need to understand the different mechanisms that interplays between the dye and the electrolyte, especially when it is applied to dyes, which have various heteroatoms at the π-conjugation bridge.

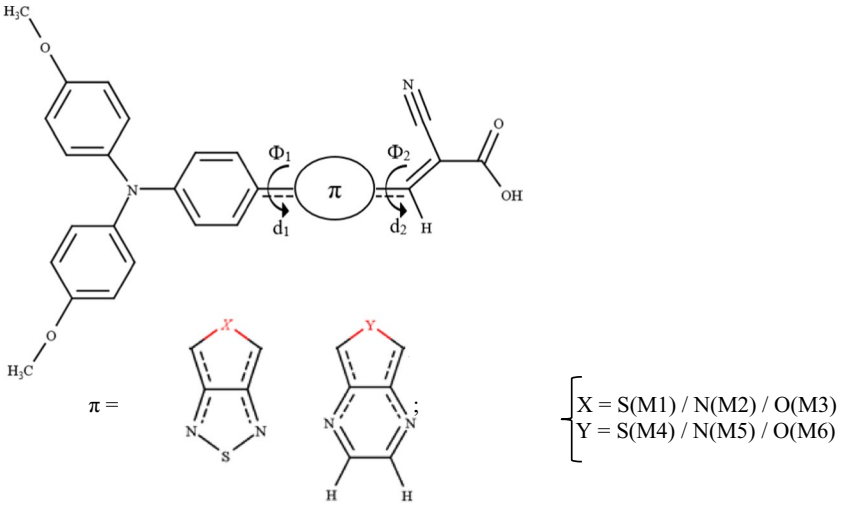

Fig. 1 Molecular structures and abbreviated notations of all studied dyes

Computational methods

Theoretical background

The power conversion efficiency, denoted η, is an important indicator for evaluating the photovoltaic performance of DSSCs. It is defined as the ratio between the maximum power (P_{max}) delivered by the cell and the incident light power (P_{in}), according to Eq. (1) [56]:

$$\eta = PCE = \frac{P_{max}}{P_{inc}} = \frac{J_{SC}V_{OC}FF}{P_{inc}} \tag{1}$$

where V_{OC} is the open-circuit potential, FF is the fill factor, and J_{SC} is the short-circuit current density.

According to Eq. (1), in order to achieve higher PCE of DSSCs, J_{SC} should be as large as possible. The J_{SC} is defined by the following Eq. (2) [57]:

$$J_{SC} = \int \mathrm{LHE}\,(\lambda)\,\Phi_{inj}\eta_{coll}\mathrm{d}\lambda \tag{2}$$

where LHE is the light-harvesting efficiency, ϕ_{inj} is the electron injection efficiency and η_{coll} is the charge collection efficiency. η_{coll} can be regarded as a constant. Based on Eq. (2), it is obvious that the larger LHE (λ) and ϕ_{inj} is beneficial to improve J_{SC} and PCE. The LHE can be obtained as followed [58]:

$$\mathrm{LHE} = 1-10^{-f} \tag{3}$$

where f is the oscillator strength of the absorbed dye at the maximum absorption. ϕ_{inj} is associated with electronic injection driving force (ΔG_{inject}), which is very

useful for studying the photovoltaic performance. It can be estimated as follows in Eq. (4) [59]:

$$\Delta G^{inject} = E_{OX}^{dye*} - E_{CB}^{TiO_2} = E_{OX}^{dye} - E_{0-0} - E_{CB}^{TiO_2} \quad (4)$$

where E_{OX}^{dye*} is the oxidation potential energy of the dye in the excited state, E_{OX}^{dye} is the redox potential energy of ground state of the dye, $E_{0\text{-}0}$ is vertical excitation energy and E_{CB}^{TiO2} is the conduction band energy of TiO_2 (−4.0 eV) [60]. The dye's ground state oxidation potential can be estimated as follows in Eq. (5) [61]:

$$E_{OX}^{dye} = -E_{HOMO} \quad (5)$$

Besides the J_{SC}, the η of DSSCs is also determined by V_{OC}, which can be described by [62]:

$$V_{OC} = \frac{E_{CB} + \Delta E_{CB}}{q} + \frac{K_b T}{q} \ln \frac{n_c}{N_{CB}} - \frac{E_{redox}}{q} \quad (6)$$

where E_{CB} represents the conduction band of the semiconductor, q is the unit charge, k_bT is the thermal energy, n_c is the number of electrons in the conduction band, N_{CB} is the accessible density of conduction band state, E_{redox} is the electrolyte Fermi level, and ΔE_{CB} is the shift of E_{CB} when the dye is adsorbed on the semiconductor. It can be calculated as the following Eq. (7) [63]:

$$\Delta E_{CB} = -\frac{q\mu_{normal}\gamma}{\varepsilon_0 \varepsilon} \quad (7)$$

here, μ_{normal} is the dipole moment of the dye, γ is the molecular surface concentration, ε_O and ε represent, respectively, the permittivity of the vacuum and the dielectric.

The open-circuit potential (V_{OC}) can be theoretically calculated as the energy difference between the LUMO level of the dye and the conduction band of the semiconductor (TiO_2) [64].

$$V_{OC} = E_{LUMO} - E_{CB}^{TiO_2} \quad (8)$$

Computational details

All calculations were performed with Gaussian 09 program [65]. The ground state geometries for all dyes were carried out by using density functional theory (DFT) method in conjunction with hybrid Becke three-parameter and Lee–Yang–Parr functional (B3LYP), which is selected for the best performance of geometry optimization [66, 67] and 6-31G(d,p) basis set. Some parameters can be obtained from the optimized configurations, including bond lengths, dihedral angles and energies of frontier molecular orbitals. Moreover, the anionic and cationic states of dyes were calculated to evaluate ionization potentials, electron affinities and reorganization

energies with the same level of theory. The BHandHLYP functional in conjunction with 6-31G + (d) basis set was used to calculate the absorption wavelengths (λ_{max}), oscillator strength (f) and excitation energies ($E_{0\text{-}0}$) for all studied dyes. The solvent effects were considered using the Conductor-like Polarizable Continuum Model (C-PCM) for tetrahydrofuran (THF). The choice of BHandHLYP functional is due to the effect of being regarded as the most stable and more reasonable method to describe absorption spectra and is widely used in the theoretical research [67]. To investigate dye-iodine and dye-TiO_2 intermolecular interactions, extra DFT calculations were performed by the B3LYP functional using the Los Alamos National Laboratory double zeta (LANL2DZ) basis set for Ti and I atoms.

Results and discussions

Molecular design and geometrical structures

All the molecular geometries of the studied molecules have been obtained with the B3LYP/6-31G(d, p) level of theory. The optimized geometry parameters of the studied dyes in the ground state are listed in Table 1 and illustrated in Fig. 2. In the D-π-A molecules, the π-spacer is used as the bridge of intramolecular charge transfer (ICT), so, the bridge bonds between donor (A) and π-spacer (L_1), and acceptor (D) and π-spacer (L_2) are calculated and discussed.

In order to indicate the molecular planarity clearly, two parameters were introduced: Φ_1, Φ_2. Here, Φ_1 is the dihedral angle between Donor and π-spacer, while Φ_2 is the dihedral angle between Acceptor and π-spacer.

Table 1 shows that Φ_1 vary in the range of 0.218 to 8.998°, while the values of Φ_2 vary between 7.261° and 23.958°. The dyes M1, M2, M4 and M5 have almost same values of Φ_2. However, M3 and M6 present, respectively, the values of 7.261° and 13.634° for Φ_2, which is may be due to the furan unit present in the π-bridge. Thus, the linked furan unit in FT and FP is favorable to the charge transfer from donor to acceptor unit, leading to an effective injection into the conduction band of TiO_2 through the cyanoacrylic acid group [68].

On the other hand, the dihedral angle Φ_1 has very low values for all dyes. However, the dyes with the thiadiazole motif show a slight effect of conjugation for the

Table 1 Selected dihedral angles Φ (◦) and bond lengths L (Å) of studied molecules at B3LYP/6-31G(d,p) level

Dyes	Φ_1	Φ_2	L_1	L_2
M1	0.755	18.351	1.440	1.415
M2	0.319	17.313	1.442	1.412
M3	0.218	7.261	1.428	1.406
M4	6.111	23.958	1.451	1.426
M5	8.998	19.298	1.450	1.417
M6	1.433	13.634	1.436	1.408

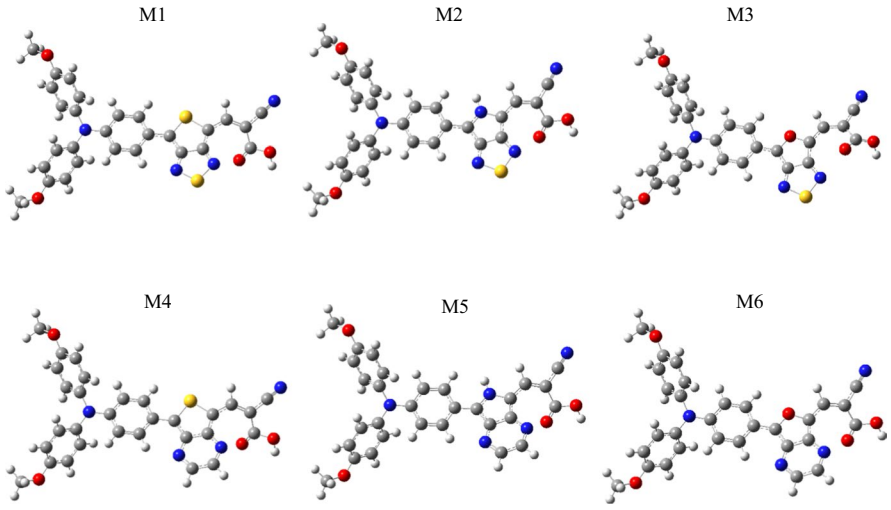

Fig. 2 Optimized geometries of studied molecules at B3LYP/6-31G(d,p) level

M1, M2 and M3 dyes, which favors a planar structure. This may be due to the charge transfer between triphenylamine and the thiadiazole fragments.

We report in Table 1 the values of bond length (L_1 and L_2) from all optimized molecules. The bonds are in the range of 1.406–1.451 Å. These results show that the bond lengths are almost the same for all dyes. However, the low values of d_2 show that the connection between donor moieties (D) and acceptor moieties (A) via π-bridge is crucial as it enhances the (ICT) character. These inter-ring distances undergo a slight increase in the case of M4 at 1.451 Å for L_1 and 1.426 Å for L_2, and in the case of M5 at 1.450 Å for L_1 and 1.417 Å for L_2. The small increase is due to the low charge transfer between the nitrogen of the pyrazine unit and the neighboring carbons. On the other hand, the bond lengths in M3 and M6 dyes are significantly decreased in comparison with other dyes. This short bond distances calculated indicate intramolecular interactions, which gives rise to molecules in a quasi-planar structure ($\Phi_1 = 0.218°$ / $\Phi_2 = 7.261°$ for M3 and $\Phi_1 = 1.433$ / $\Phi_2 = 13.634°$ for M6) and facilitates the electron delocalization over the whole molecular system under optical excitation.

Frontier molecular orbitals and energy levels

To discover the effect of the π-bridge on the electronic properties of the studied dyes for use in DSSCs, we presented in Fig. 3 the highest occupied molecular orbital (HOMO), the lowest unoccupied molecular orbital (LUMO) and gap energy (E_{gap}) values of all the studied dyes.

As shown in Fig. 3, the HOMO energies of all studied dyes are in the range of (−5.04)–(−4.87) eV, while the LUMO level, which is more affected by the different electron π-conjugation linkers, increases in the following order: M3 < M1 < M4 < M6 < M2 < M5. Thus, it is clear that the LUMO levels of

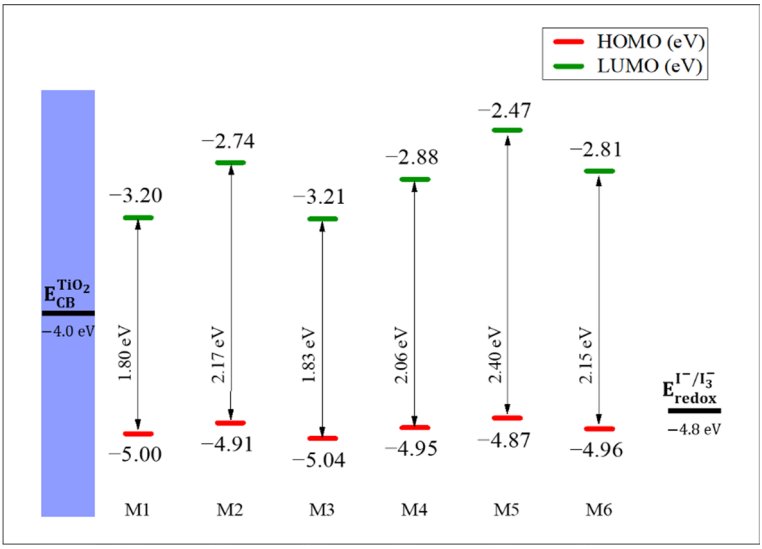

Fig. 3 Schematic diagram of calculated energy HOMO and LUMO levels for the studied dyes, along with CB of TiO_2 and redox potential of I^-/I_3^-

thiadiazole, thiophene and furan π-conjugated system based dyes are much lower than that of dyes based on pyrazine and pyrrol units, suggesting that the charge-transport ability of the π-conjugated system based on heterocycles with sulfur or oxygen atoms was much stronger than that of nitrogen based heterocycles. Moreover, the E_{gap} of these dyes increase in the order M1 < M3 < M4 < M6 < M2 < M5. The results indicate that the dyes M1, M3 and M4 exhibit the best electronic properties due to their narrow gap energies when compared with other molecules; in particular, M1 has the stronger electron π-conjugated system, which leads to narrow HOMO–LUMO gap energies.

Moreover, the substitution of the pyrazine unit by the thiadiazole unit leads to a decrease from 2.06 to 1.80 eV for M4/M1, from 2.40 to 2.17 eV for M5/M2, and from 2.15 to 1.83 eV for M6/M3. The addition of thiadiazole unit in dyes M1, M2 and M3 effectively lowered their LUMOs compared with that of M4, M5 and M6. Due to the significant decrease in the LUMO level, the gap energies of thiadiazole-based dyes are smaller than that of pyrazine-based dyes. Therefore, the thiadiazole unit is expected to be a stronger electron-deficient group, which may be due to the Coulombic interaction between sulfur and oxygen atoms [69].

On the other hand, as shown in Fig. 4, for the HOMO level, the electron density is located over the molecule and mainly located on the triphenylamine and π-spacer units, the bonding orbitals are located on the bridging C = C atoms, while the anti-bonding orbitals are located on the bridging CC atoms. For the LUMO level, the electron density is located on the acceptor units and part of the π-bridge, which form the π-rich part. The distributions of the electron density of the HOMO and LUMO indicate that an excited electron moves from the TPA donor to the cyanoacrylic acid acceptor via the π-bridge group, ensuring

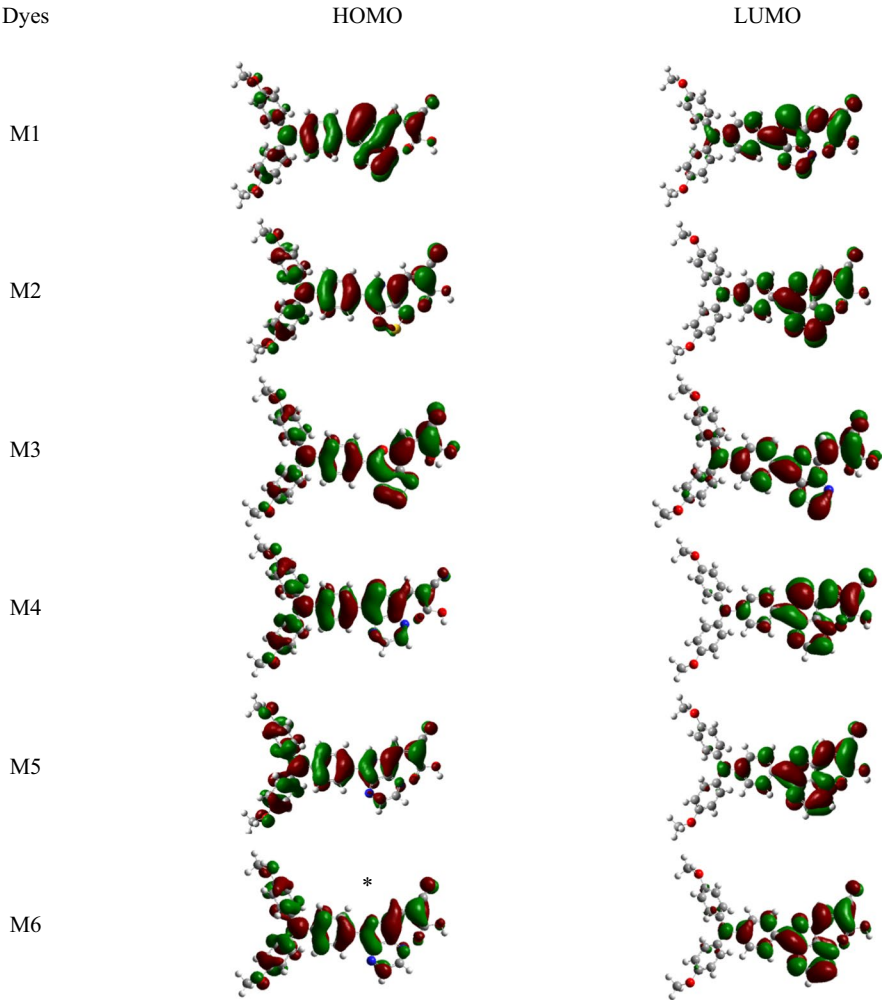

Fig. 4 Distribution of molecular orbital (HOMO and LUMO) of the studied dyes, obtained at B3LYP 6-31G(d,p) level of theory

efficient charge separation and electron injection. This transition can be classified as a π–π* ICT [70].

Understanding the energy levels of the dyes is most important to explain the electron injection and charge regeneration process in DSSCs. For this reason, the energy level diagram of the HOMOs and LUMOs are presented in Fig. 3. We note that all dyes have sufficiently high E_{LUMO} and are energetically favorable for electron injection into the conduction band of TiO_2 (−4 eV) [71]. On the other hand, the HOMO level of the dyes M1-M6 occurs in the range (−5.04 eV) at (−4.87 eV) which was more positive to that of I^-/I_3^- redox electrolyte (−4.80 eV) [72]. This is a sufficient thermodynamic condition for efficient dye regeneration by I^-/I_3^- redox couple.

The electrochemical data confirm the existence of driving force for electron injection into the conduction band of TiO_2 and regeneration of dyes by I^- in the electrolyte.

Natural bond orbital (NBO) analysis

In order to analyze charge populations on D-π-A dyes, the Natural Bound Orbital (NBO) analysis provides a practical basis for charge distribution and electron transfer in D-π-A systems. This analysis was performed at B3LYP/6-31G(d, p) level, and the values are listed in Table 2. The positive NBO charge of donor and π-spacer units for all dyes reveals that they are effective electron-pushing units. Contrarily, the negative NBO values of acceptor units indicate that they will efficiently receive the electrons transferred from the electron donor part. During the photo-excitation, the NBO charges on the donor for all dyes are in following order; M1 (0.176) > M3 (0.173) > M2 (0.165) > M4 (0.139) > M6 (0.131) > M5 (0.072), indicating that dyes with thiadiazole-based bridges have strong electron-donating capability than that of dyes with pyrazine unit. For the acceptor, the NBO charges show that the introduction of thiadiazole derivatives as units in π-spacer can increase the density of electrons in the acceptor. Moreover, the charge in the acceptor group of M3 dye indicate that furano-thiadiazole (FT) as a π-spacer could greatly favor charge transfer as it shows an effective electron-withdrawing unit.

Electronic absorption spectra

As we know, light absorption ability inevitably influence on J_{SC}, thus, dye with a great capability to absorb solar radiation is beneficial to improve efficiency of devices. The optical properties of dyes with different π-spacers were carried out by TD-BHandHLYP-/6-31G + (d) level in THF solution. The vertical transition energies ($E_{0\text{-}0}$), oscillator strengths (f), maximum absorption wavelengths (λ_{max}) and main transition transitions are listed in Table 3.

The maximum absorption wavelengths (λ_{max}) are in following order: M1 (738 nm) > M3 (639 nm) > M2 (537 nm) > M4 (528) > M6 (525 nm) > M5 (473 nm). The introduction of thiadiazole moiety reveals strong effects on the maximum absorption wavelengths and leads to remarkably red-shifted adsorption bands for M1, M2 and M3 when compared to M4, M5 and M6 pyrazine-based dyes; this may

Table 2 Natural Bond Orbital analysis (atomic charge in a.u) of the studied dyes

Dyes	Donor	π-spacer	Acceptor
M1	0.176	0.029	−0.208
M2	0.165	0.129	−0.214
M3	0.173	0.059	−0.227
M4	0.139	0.016	−0.156
M5	0.072	0.138	−0.210
M6	0.131	0.076	−0.203

Table 3 Calculated excitation energies ($E_{0\text{-}0}$/eV), maximum absorption wavelengths (λ_{max}/nm), oscillator strengths (*f*), Light-harvesting efficiencies (LHE) and electronic transition configurations for all studied dyes in tetrahydrofuran (THF) solvent, at the TD-BHandHLYP/6-31G + (d) level (H stands for HOMO and L for LUMO)

Dyes	$E_{0\text{-}0}$(eV)	λ_{max} (nm)	*f*	LHE	Main transitions
M1	1.678	738	0.664	0.783	H L (69%) H – 1 L (12%)
M2	2.307	537	0.868	0.865	H L (69%) H – 1 L (13%)
M3	1.940	639	0.702	0.801	H L (69%) H – 1 L (12%)
M4	2.344	528	0.952	0.888	H L (67%) H – 1 L (18%)
M5	2.620	473	1.027	0.906	H L (67%) H – 1 L (18%)
M6	2.360	525	0.956	0.889	H L (68%) H – 1 L (17%)

be due to the thiadiazole unit, which is much stronger π-electron deficient unit. In the case of M1, the incorporation of the thiadiazole with thiophene units displays a remarkable nearly 100 nm red-shifting absorption than M3. The dye M1 has presented a low E_{gap}, which results to a red-shifted adsorption. This is ascribed to the transition absorption of intramolecular charge transfer (ICT) from the triphenylamine donor to cyanoacrylic acid acceptor through the thienothiadiazole π-spacer [73].

Dyes M1 and M4 with thiophene-based spacers, displays a red-shifted absorption band when compared to dyes with pyrrole and furan units. This contributes to the better conjugation leading to more efficient intramolecular charge transfer. Therefore, M1 and M4 show the red-shifted ICT absorption and absorb more photons from the visible region, indicating their superior light-harvesting ability in comparison with M2, M3, M5 and M6 dyes based on pyrrole and furan bridges. This may be attributed to the smaller resonance energy of the furan than thiophene, which ensures a more effective conjugation in the π-bridge of M1 or it may be caused by the lower electronegativity of the sulfur atom present in thiophene.

We can conclude from Table 3 that the main absorption band of all studied dyes mainly corresponds to the HOMO to LUMO transition. Moreover, from Fig. 5, we note that the studied dyes exhibit two main absorption bands. The first band of lower intensity between 300 and 400 nm which could be attributed to the electronic transfer $\pi \rightarrow \pi^*$[74]. The second band of highest intensity between 400 and 800 nm, which could be attributed to the intramolecular charges transfer [74].

From the results above, we can conclude that π-bridge has a considerable influence on the light-harvesting ability of these triphenylamine-based dyes.

The oscillator strength (*f*) is another parameter that communicates the probability of electromagnetic radiation absorption by transitions between the energy levels of an atom or molecule. The oscillator strength values of these dyes at the maximum absorption are presented in Table 3, revealing values in the range of 0.664–1.027 and show the same trend as the λ_{max} peaks.

According to Eq. (2), the light-harvesting efficiency (LHE) is an important factor affecting the J_{SC}. Generally, a high LHE is needed to get a maximum photocurrent.

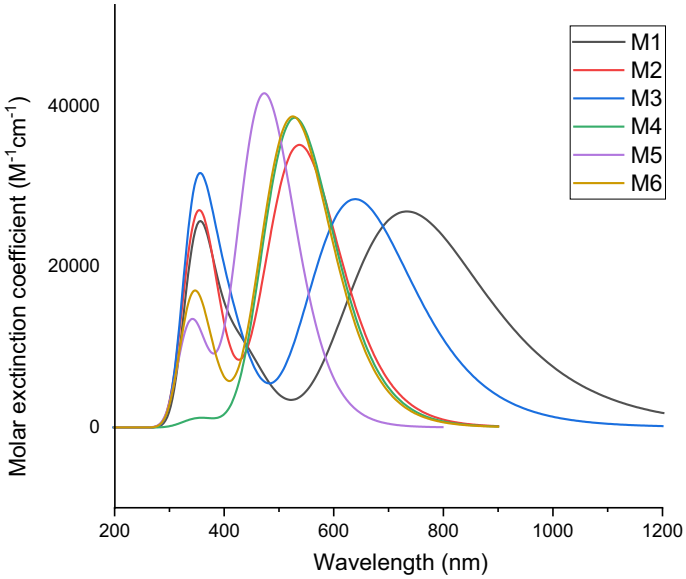

Fig. 5 Simulated absorption spectra of the Mi (i = 1–6) molecules, calculated at TD-BH and HLYP/6-31G + (d) level of theory in THF solution

Among all dyes, M5 displays largest LHE (0.906), followed by M6 (0.889) and M4 (0.888). These results indicate that the substitution with pyrazine groups is a useful way to enhance the photo current response.

Injection and transport of the charge carriers

The design of DSSCs requires an efficient and balanced injection and transport of holes and electrons. Within this framework, ionization potentials (IP), electron affinities (AE), electron extraction potentials (EEP) and hole extraction potentials (PET) were calculated as described in our previous study Lazrak et al., 2020 [70]. We note that a low IP and a high EA are beneficial to facilitate hole and electron injection in photosensitive dye materials [75]. Table 4 presents the ionization potentials (IPa / IPv), electron

Table 4 Calculated vertical and adiabatic values of IP and EA, hole and electron extraction potentials (HEP and EEP) and reorganization energies of studied dyes (in eV)

Dyes	IPa	IPv	EAa	EAv	HEP	EEP	λ_h	λ_e	λ_{total}
M1	5.942	6.039	2.157	1.945	5.849	2.381	0.189	0.437	0.626
M2	5.873	5.975	1.695	1.455	5.772	1.992	0.203	0.537	0.741
M3	5.897	6.093	2.145	1.922	5.848	2.381	0.245	0.459	0.704
M4	5.902	6.009	1.872	1.633	5.801	2.118	0.207	0.486	0.693
M5	5.832	5.946	1.451	1.203	5.724	1.725	0.222	0.522	0.744
M6	5.917	6.022	1.785	1.545	5.818	2.035	0.203	0.490	0.694

affinities (EAa / EAv), hole and electron extraction potentials (HEP / EEP) calculated at B3LYP/6-31G(d, p) level of theory.

As shown in Table 4, M5 and M2 exhibit the lower IPa/IPv (5.832/5.946 eV) and (5.873/5.975 eV), respectively. This may be attributed to the introduction of pyrrole in the first π-spacer part, especially in M5 having the lowest IP, which is clearly explained by the introduction of the pyrrole and the pyrazine units in π-spacer, thereby improving the carrier injection ability. As a result, dyes with nitrogen based spacers have superior hole injection capability compared to other dyes.

For EA, the results show that M1 and M3 dyes require high energy (EAa/EAv), which suggest that thiadiazole-based dyes are more favorable for injecting an electron directly to the TiO_2 semiconductor.

The hole and electron extraction potentials HEP and EEP of the studied dyes exhibit the same trend as described for IP and EA, respectively.

Furthermore, the reorganization energy (λ_{total}) in an important parameter, which affects the performance of DSSC device. It can be expressed as:

$$\lambda_{total} = \lambda_e + \lambda_h \tag{9}$$

We note that the smaller total reorganization energy will accelerate electron transfer. λ_{total} is consisted of electron and hole reorganization energies (λ_h / λ_e) which are evaluated from the following formulas [31]:

$$\lambda_h = \left[E^+(M) - E(M)\right] - \left[E^+\left(M^+\right) - E\left(M^+\right)\right] \tag{10}$$

$$\lambda_e = [E(M^-) - E^-(M^-)] - [E(M) - E^-(M)] \tag{11}$$

with, E(M), $E^+(M^+)$ and $E^-(M^-)$ are, respectively, the energies of the neutral, cation and anion species in their ground state geometries. $E^+(M)$ and $E^-(M)$ represent, respectively, the energies of the cation and anion species with the geometries of the neutral species. $E(M^+)$ and $E(M^-)$ represent the energies of the neutral species with the geometries of the cation and anion species, respectively.

According to the values of the hole and electron reorganization energies listed in Table 4, the values of λ_h are less than those of λ_e for all dyes; it indicates that these organic molecules are more appropriate for hole-transport materials.

The more balanced is the reorganization energy between hole and electron, the greater luminous efficiency will be found for the studied dyes [76]; M1 has the lowest total reorganization energy, which reflects its most favorable charge-transport properties.

These results indicate that the introduction of thiophene and thiadiazole as units in π-bridge is appropriate for generating and transporting free holes and electrons as the p-type materials in organic solar cell devices, which is due to their electron-rich properties and small volume.

Important factors related to the photovoltaic performance of DSSCs

In order to seek out the influence of different π-spacers on the efficiency, various key parameters including the free energy of charge injection (ΔG^{inject}), free energy of charge injection of dye regeneration (ΔG^{reg}) and dipole moment (μ_{normal}) are used to evaluate short-circuit current density (J_{SC}) and open-circuit voltage (V_{OC}), and the corresponding data are tabulated in Table 5. According to Eq. (2), free energy of charge injection (ΔG^{inject}) is important factor affecting the J_{SC}. The negative ΔG^{inject} value means that electrons can be injected into TiO_2 semiconductor. The lower ΔG^{inject} is beneficial to increase J_{SC}. The results show that dyes with pyrazine unit are more negative than thiadiazole-based dyes, which means that they will have larger J_{SC}. Moreover, the ΔG^{inject} value calculated for all the studied molecules increases in the order M5 < M6 < M4 < M2 < M3 < M1.

On the other hand, the free energy of charge injection of dye regeneration (ΔG^{reg}) is another factor which affects the efficiency of DSSCs, it can be estimated by the following Eq. (12) [31]:

$$\Delta G^{reg} = E_{OX}^{dye} - E_{redox}^{I^-/I_3^-} \tag{12}$$

where $E_{redox}^{I^-/I_3^-}$ is the redox potential energy level of the couple I^-/I_3^-. High ΔG^{reg} is required to achieve the fast electron transfer [77]. As shown in Table 6, the ΔG^{reg} value of M5 dye is higher than that of the others dyes.

The results above reveal that dye M5 with pyrrolo-pyrazine as π-bridge exhibits a high power conversion efficiency compared with other molecules ($\Delta G^{inject} = -1.74$ eV and $\Delta G^{reg} = -0.08$ eV)[77]. This indicate that the injection and regeneration processes are easier for the molecules possessing a nitrogen heteroatom than for those possessing a sulfur and oxygen heteroatoms.

On the other hand, the dipole moment (μ) decreases in the following order M3 (17.28 D) > M1 (15.20 D) > M2 (14.08 D) > M4 (12.84 D) > M6 (12.70 D) > M5 (12.17 D). According to Eqs. (6) and (7), this variation can explain the higher estimated V_{OC} value observed for M1 and M3 dyes compared to the other studied molecules. On the other hand, the high value of V_{OC} measured for the dye M3 is due to the low energy of the HOMO orbital, which increases the value of $|\Delta G^{reg}|$.

Table 5 Free energies of charge injection ΔG^{inject} and dye regeneration ΔG^{reg}, estimated open-circuit voltage V_{OC} and dipole moment μ of the studied molecules

Dyes	ΔG^{inject} (eV)	ΔG^{reg} (eV)	μ(Debye)	V_{OC} (eV)
M1	−0.68	−0.20	15.203	7.20
M2	−1.39	−0.11	14.076	6.74
M3	−0.89	−0.24	17.284	7.21
M4	−1.39	−0.15	12.843	6.89
M5	−1.74	−0.08	12.170	6.48
M6	−1.39	−0.16	12.704	6.81

Table 6 Calculated interactions Energies (kcal/mol), distances (Å) and angles (°) for the Various Dye-I_2 Adducts

Mi (i = 1–6)-I_2	Adduct	Distance (Å)	Angle (°)	ΔE (kcal/mol)
M1	S-I_2	I-S / 5.165	S-I-I / 126.2	−3.78
		I-I / 2.882		
	CN-I_2	I-N / 3.076	CN-I-I / 179.2	
		I-I / 2.873		
M2	S-I_2	I-S / 3.981	S-I-I / 165.5	−3.23
		I-I / 3.019		
	CN- I_2	I-N / 2.637	CN-I-I / 177.5	
		I-I / 2.974		
M3	S-I_2	I-S / 3.423	S-I-I / 167.1	−3.26
		I-I / 3.005		
	CN-I_2	I-N / 2.635	CN-I-I / 177.1	
		I-I / 2.964		
M4	S-I_2	I-S / 3.544	S-I-I / 151.8	−3.27
		I-I / 3.113		
	CN-I_2	I-N / 2.733	CN-I-I / 179.5	
		I-I / 2.911		
M5	N-I_2	I-N / 3.963	N-I-I / 179.1	−2.72
		I-I / 2.993		
	CN-I_2	I-N / 2.708	CN-I-I / 176.8	
		I-I / 2.928		
M6	O-I_2	I-O / 4.111	O-I-I / 136.9	−2.75
		I-I / 2.918		
	CN-I_2	I-N / 3.503	CN-I-I / 42.7	
		I-I / 2.902		

Dye-I_2 ground state structures

Recently a number of experimental and computational studies have been focused on the interactions between the oxidized dyes and electrolyte and their implications in the dye regeneration mechanism. For most DSSCs, an iodide/triiodide (I^-/I_3^-) redox couple is employed as an electrolyte [78, 79]. However, we need to understand the different mechanisms that interplays between the dye and the electrolyte, especially when it is applied to dyes having various heteroatoms at the π-conjugation bridge. Otherwise, the regeneration reaction proceeds via the formation of I_2^-[78]:

$$Dye^+ + 2I^- \rightarrow Dye + I_2^-$$

I_2^- then dismutates to yield iodide and triiodide:

$$2\,I_2^- \rightarrow I^- + I_3^-$$

We studied the dye-iodine interactions sites of the dyes M1-M6:

- The cyano group of cyanoacrylic acid (CN-I_2 interaction) in Mi dyes (i = 1–6);
- The sulfur atom of thiadiazole (S-I_2 interaction) in M1, M2 and M3;
- The sulfur atom of thiophene (S-I_2 interaction) in M4;
- The pyrrole nitrogen atom (N-I_2 interaction) in M5;
- The furan oxygen atom (O-I_2 interaction) in M6.

The optimized molecular structures of different interactions of the Mi (i = 1–6) dyes with I_2 and the corresponding total energies are shown in Fig. 6. The I-X distances (with X = O, S and N), the I-I distances and the X-I-I angles (with X = O, S, CN and N) are listed in Table 6. As shown in Fig. 6, I_2 interactions to sulfur, oxygen and nitrogen atoms with different geometric arrangements is coplanar with the molecule in the case of the N-I_2 with CN-I-I and N-I-I, except for the molecule M6.

Whereas iodine molecular is perpendicular to the dye in case of sulfur and oxygen atoms. Furthermore, it can be noted that the total energies of the dye-I_2 systems of all studied dyes are negatives, revealing a favorable interaction with I_2. The obtained total energies (in eV) are in the intervals of [(− 606.88)–(− 619.26)] and [(− 606.88)–(− 619.31)] for the S-I_2 adduct (sulfur of thiadiazole) and CN-I_2, respectively, and in the order of (− 619.15), (− 619.27) and (− 619.32) for the adducts S-I_2 (sulfur of thiophene), N-I_2 (nitrogen of pyrrole) and O-I_2 (oxygen of furan), respectively. Analysis of these results shows that the total energies of the dyes with CN-I_2 adduct are more negative than those of the other adducts, which suggests that the interactions of iodine species with the nitrogen of the cyano moiety are more favorable compared to other interactions. This result may be due to non-covalent I-N bond, which are much stronger than I-S and I-O interactions, thereby suggesting nitrogen as a better electron donor.

On the other hand, interactions energies (ΔE) was determined by the energy difference between the dye-I_2 complex and the sum of the isolated monomers [80]. Moreover, a smaller (more negative or less positive) ΔE value indicates a stronger intermolecular interaction.

For the studied complexes, we can note that the absolute value of the interactions energies of the dye-I_2 interactions increases in the following order: M5 < M6 < M2 < M3 < M4 < M1. Therefore, we can conclude that the concentration of iodine nearby the M1 dye, where electronic recombination occurs in the electrolyte, is lower than that of other dyes.

The data reported in Table 6 show a comparable difference between CN-I_2, S-I_2 and O-I_2 adducts. the lower values of the I-X bond distance (with X = O, S and N) are attributed to CN-I_2 interactions with I–N distances that vary from 2.635 to 3.503 Å, confirming that the CN group is the most appropriate site for the formation of the dye–iodine complex by interaction [81].

Indeed, the distances from the CN interaction site (CN-I_2) are smaller than the Van der Waals radii (3.78 Å) [82]. These shorter distances prove strong halogen interaction. Compared to the isolated I_2 bond (2.833 Å) [82], the intramolecular I-I bonds in the dye-iodine systems are larger, indicating that I-I bonds weaken upon interaction with the dye. The intramolecular I-I bond lengths for all interactions of the studied complexes are longer than the covalent radii (2.03 Å) [83]. These results

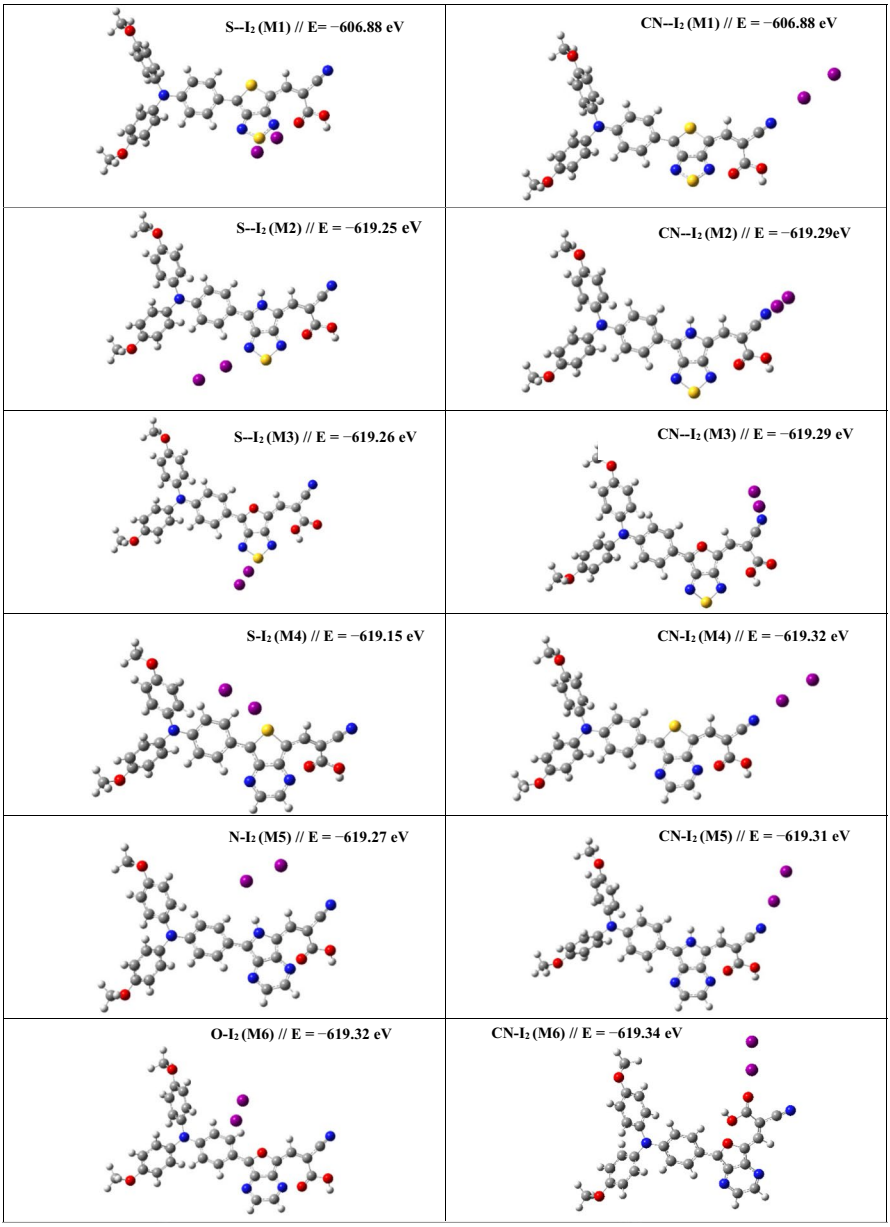

Fig. 6 Optimized molecular structures of the studied dyes-I_2 adducts. Iodine atoms are in purple, carbon in gray, sulfur in yellow, nitrogen in blue, oxygen in red, and hydrogen in white

reveal that all the studied dyes form an intermolecular charge transfer complexes with I_2.

Furthermore, we can note that the distances of M1 molecule are in the order of 5.165 and 3.076 Å for I-S and I-N bonds, respectively. For M2 dye based on

pyrrolo-thiadiazole spacer, we observe a slight increase in the bond lengths, which are in order of 3.981 and 2.637 Å, respectively, for the I-S and I-N bonds. A similar trend is observed for the dye M3, where the CN-I_2 and S-I_2 interactions become stronger compared to those of the other dyes, as the distances of the I-S and I-N bonds become shorter. These results indicate that the intermolecular interactions of I_2 with M3 are stronger than those with the other dyes studied, which is due to the effect of the furano-thiadiazole group as a π-spacer.

Therefore, the M1 and M3 dyes might have a potential to delay the charge recombination process. These results are confirmed by the improved values of μ_{normal}, and V_{OC} observed for M1 and M3 (Table 5), showing the strong interaction between the dyes and iodine, which disadvantages the phenomenon of recombination.

Adsorption of M1 and M3 dyes on $(TiO_2)_9$ cluster

The overall efficiency and stability of dye-sensitized solar cells is significantly dependent on adsorption of the dye onto the semiconductor surface [84]. In this part, we are interested in dyes M1 and M3 since they present the best optoelectronic properties with an efficient generation and transfer of free holes and electrons and a higher estimated open-circuit voltage V_{OC}. We have adopted the $(TiO_2)_9$ cluster to represent the surface of the TiO_2 semiconductor due to its balanced electronic properties [85]. The carboxylates of the dyes bond with the Ti atoms on the TiO_2 surface. There are generally three binding modes, including monodentate, bidentate chelate, and bidentate bridged binding [86]. For an organic dye with a carboxylic acid as an electron acceptor, a bidentate chelate bond should be energetically favorable [87]. Therefore, the bidentate chelate bonding mode was adopted in the study of dye@$(TiO_2)_9$ complexes.

The methodology adopted to study the complexe dye@$(TiO_2)_9$, is based on the B3LYP functional using the 6-31G(d, p) base for non-metals (C, H, O, S, N) and (LANL2DZ) for titanium atoms. The optimized structures of the dyes adsorbed on the surface $(TiO_2)_9$ are presented in Fig. 7. The main geometrical parameters of the systems M1, M1@$(TiO_2)_9$, M3 and M3@$(TiO_2)_9$ in particular the bonds lengths and the angles, are given in Table 7.

From Fig. 7, we can notice that after adsorption on the $(TiO_2)_9$ cluster, the sensitizers dyes almost keep their structures, except for the cyanoacrylic group, which acts as a ligand with TiO_2. Furthermore, it can be seen from Table 7, that the structural parameters change from isolated M to M@TiO_2 system. The S-C_1 and C_4-O_3 distances for adsorbed systems adopt a more relaxed geometry than when M1 and M3 are isolated. While, the distances O_1-C_1 and C_1-C_2, for adsorbed systems, are shorter than when M1 and M3 are isolated.

Thus, a slight variation is observed for the lengths of the other bonds. The Ti_1-O_2 bonds are 2.020 and 2.033 Å for M1@TiO_2 and M3@TiO_2, respectively, depending on the π-bridge used. The second distance, Ti_1-O_3, is slightly longer (2.080 and 2.087 Å for M1@TiO_2 and M3@TiO_2, respectively). These values indicate that the studied dyes exhibit a strong chemisorption at the TiO_2 surface.

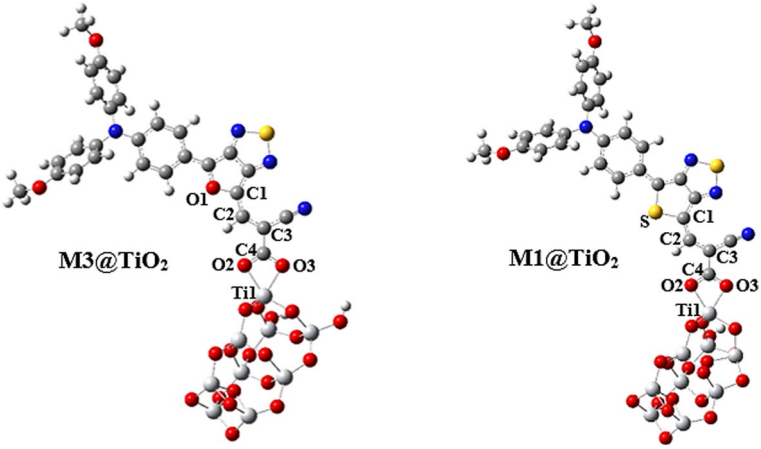

Fig. 7 Optimized structures of the M1@TiO_2 and M3@TiO_2 systems, calculated by B3LYP using the 6-31G(d, p) basis for non-metals and the LANL2DZ basis for Ti atoms

Table 7 Main geometric parameters (Distances in (Å) and angles in (°)) of the M1, M3, M1@TiO_2 and M3@TiO_2 systems, calculated by B3LYP using the 6-31G(d, p) basis for non-metals and the LANL2DZ basis for Ti atoms

Distance/Angle	M1	M1@TiO_2	M3	M3@TiO_2
S-C_1	1.760	1.768	–	–
O_1-C_1	–	–	1.402	1.343
C_1-C_2	1.415	1.401	1.406	1.424
C_4-O_2	1.214	1.292	1.214	1.292
C_4-O_3	1.356	1.284	1.355	1.284
Ti_1-O_2	–	2.020	–	2.033
Ti_1-O_3	–	2.080	–	2.087
S-$C_1C_2C_3$°	161.6	179.3	–	–
$O_1C_1C_2C_3$°	–	–	172.7	179.6
$O_3C_4O_2$°	122.5	114.7	122.9	115.1
$Ti_1O_2C_4$°	–	91.90	–	91.69

The adsorption energy is used to evaluate the stability and the interaction between sensitizer dye and semiconductor surface [86]. The adsorption energy is calculated according to the following expression:

$$E_{ads} = E_{Dye-TiO_2} - \left(E_{Dye} + E_{TiO_2}\right) \quad (13)$$

where, $E_{Dye-TiO_2}$ represents the total energy of dye@TiO_2 complexe, E_{Dye} is the total energy of the isolated dye and E_{TiO_2} represents the total energy of $(TiO_2)_9$ cluster. The total energy of $(TiO_2)_9$ cluster was found to be − 1878.4956 a.u. The calculated adsorption energies (E_{ads}) are listed in Table 8.

The adsorption energy is in the order of − 5.10 eV and − 22.17 eV for M1 and M3, respectively. These negative values indicate a stable adsorption and are important to confirm that the adsorption on the surface of TiO_2 is favorable for M1 and

Table 8 The calculated adsorption energies of M1@$(TiO_2)_9$ and M_3@$(TiO_2)_9$ systems

Mi@TiO_2	$E_{Dye-TiO_2}$, a.u	E_{Dye}, a.u	E_{ads}, eV
M1	− 4273.9329	− 2395.2498	− 5.10
M3	− 3951.5812	− 2072.2705	− 22.17

M3 dyes. Furthermore, the M3 dye exhibits a higher adsorption energy compared to its M1 counterpart. Thereby, the furano-thiadiazole π-spacer contributes to an increase in binding energy at the surface of $(TiO_2)_9$ cluster. These results indicate that the adsorption of M3 onto the TiO_2 semiconductor would be more stable.

Conclusions

In summary, six triphenylamine-based organic dyes (M1-M6) with different π-conjugated spacers based on thiadiazole and pyrazine units were designed. The strucrural, electronic, absorption spectra, and factors related to the photovoltaic performance of DSSCs of studied dyes were investigated via DFT and TD-BH and HLYP calculations, with the aim of identifying sensitizers with high performance for use in DSSCs.

The results reveal that the M1 and M3 dyes exhibit a lower level of LUMO energy, which consequently decreases the E_{gap} by revealing remarkable effects on the maximum absorption wavelengths. In addition, the charge transfer characteristics of these dyes are significantly improved. The M1 and M3 dyes exhibit higher V_{OC} values compared to the other dyes, which contributes to a significant increase in photoelectric conversion efficiency.

On the other hand, the improved free energies of charge injection (ΔG^{inject}) and light-harvesting efficiency values of dye M5 based on pyrrolo-pyrazine unit revealed that this dye could achieve distinctly higher J_{SC}.

For the dye-iodine interactions, the binding energies were in good correlation with the open-circuit voltage of the dyes. This suggesting the increase in the concentration of iodine near the vicinity of the surface of the semiconductor, which disadvantages the phenomenon of recombination that affects the solar cell efficiencies. Moreover, the results suggest the dyes M1 and M3 based, respectively, on thienothiadiazole and furano-thiadiazole groups show more stable interactions with iodine species, which increase the concentration of the redox couple at the surface of the semiconductor.

In addition, from the geometrical and electronic parameters obtained from the dye@TiO_2 systems, we can conclude that the adsorption of M3 dye exhibits a lower energy compared to its M1 counterpart. Thereby, we deduce a strong intramolecular charge transfer (ICT) property and more stable adsorption for dyes with furano-thiadiazole as a π-spacer.

We can conclude that M1 and M3 molecules with, respectively, thienothiadiazole and furano-thiadiazole as π-spacers can be promising sensitizers for dye solar cell applications. This is due to their excellent balance in various key properties and their

remarkable performance in adsorption and regeneration processes. Therefore, the choice of the appropriate π-bridge in dye molecule is very important for the design of new sensitizers with improved performance.

Acknowledgments Realized with the support of the National Center for Scientific and Technical Research (CNRST—Morocco) as part of the Research Excellence Awards Program (No. 28USMBA2017).

Author contributions M.L. did most of the practical work as part of a PhD thesis supervised by H.T. and prepared the manuscript. H.T. designed and coordinated the study, participated in article preparation, corrected the manuscript and edited the final version and submitted it for publication. S.E. contributed to data analysis. F.L. and S.M.B. participated in study design, helped to improve the manuscript and critically revised the manuscript. All authors read and approved the final manuscript.

Funding Polydisciplinary Faculty of Taza, Sidi Mohamed Ben Abdellah University, Taza, Morocco.

Data availability All data are available and mainly the Cartesian coordinates of all the studied dyes.

Declarations

Conflict of interest The authors declare no conflict of interests.

Ethical approval Not applicable.

References

1. M.S. Dresselhaus, I.L. Thomas, Nature **414**, 332 (2001)
2. E.W.-G. Diau, ACS Energy Lett. **2**, 334 (2017)
3. B. O'Regan, M. Grätzel, Nature **353**, 737 (1991)
4. T. Higashino, H. Imahori, Dalton Trans. **44**, 448 (2014)
5. A. Yella, C.-L. Mai, S.M. Zakeeruddin, S.-N. Chang, C.-H. Hsieh, C.-Y. Yeh, M. Grätzel, Angew. Chem. Int. Ed. **53**, 2973 (2014)
6. M. Urbani, M. Grätzel, M.K. Nazeeruddin, T. Torres, Chem. Rev. **114**, 12330 (2014)
7. W.M. Campbell, K.W. Jolley, P. Wagner, K. Wagner, P.J. Walsh, K.C. Gordon, L. Schmidt-Mende, M.K. Nazeeruddin, Q. Wang, M. Grätzel, D.L. Officer, J. Phys. Chem. C **111**, 11760 (2007)
8. T. Bessho, S.M. Zakeeruddin, C.-Y. Yeh, E.W.-G. Diau, M. Grätzel, Angew. Chem. Int. Ed. **49**, 6646 (2010)
9. S. Mathew, A. Yella, P. Gao, R. Humphry-Baker, B.F.E. Curchod, N. Ashari-Astani, I. Tavernelli, U. Rothlisberger, M.K. Nazeeruddin, M. Grätzel, Nat. Chem. **6**, 242 (2014)
10. M.-E. Ragoussi, M. Ince, T. Torres, Eur. J. Org. Chem. **2013**, 6475 (2013)
11. G.C. Vougioukalakis, A.I. Philippopoulos, T. Stergiopoulos, P. Falaras, Coord. Chem. Rev. **255**, 2602 (2011)
12. K.-M. Lee, S.-J. Wu, C.-Y. Chen, C.-G. Wu, M. Ikegami, K. Miyoshi, T. Miyasaka, K.-C. Ho, J. Mater. Chem. **19**, 5009 (2009)
13. S.-Q. Fan, C. Kim, B. Fang, K.-X. Liao, G.-J. Yang, C.-J. Li, J.-J. Kim, J. Ko, J. Phys. Chem. C **115**, 7747 (2011)
14. K. Hara, T. Sato, R. Katoh, A. Furube, T. Yoshihara, M. Murai, M. Kurashige, S. Ito, A. Shinpo, S. Suga, H. Arakawa, Adv. Funct. Mater. **15**, 246 (2005)
15. L. Kloo, Chem. Commun. **49**, 6580 (2013)
16. H. Spanggaard, F.C. Krebs, Sol. Energy Mater. Sol. Cells **83**, 125 (2004)
17. H. Chen, H. Huang, X. Huang, J.N. Clifford, A. Forneli, E. Palomares, X. Zheng, L. Zheng, X. Wang, P. Shen, B. Zhao, S. Tan, J. Phys. Chem. C **114**, 3280 (2010)
18. H. Choi, I. Raabe, D. Kim, F. Teocoli, C. Kim, K. Song, J.-H. Yum, J. Ko, M.K. Nazeeruddin, M. Grätzel, Chem. Eur. J. **16**, 1193 (2010)

19. S. Namuangruk, R. Fukuda, M. Ehara, J. Meeprasert, T. Khanasa, S. Morada, T. Kaewin, S. Jungsuttiwong, T. Sudyoadsuk, V. Promarak, J. Phys. Chem. C **116**, 25653 (2012)
20. C. Li, J.-H. Yum, S.-J. Moon, A. Herrmann, F. Eickemeyer, N.G. Pschirer, P. Erk, J. Schöneboom, K. Müllen, M. Grätzel, M.K. Nazeeruddin, Chemsuschem **1**, 615 (2008)
21. Y. Shibano, T. Umeyama, Y. Matano, H. Imahori, Org. Lett. **9**, 1971 (2007)
22. F. De Angelis, Chem. Phys. Lett. **493**, 323 (2010)
23. K. Hara, K. Sayama, Y. Ohga, A. Shinpo, S. Suga, and H. Arakawa, Chem. Commun. 569 (2001).
24. Z.-S. Wang, Y. Cui, K. Hara, Y. Dan-oh, C. Kasada, A. Shinpo, Adv. Mater. **19**, 1138 (2007)
25. K. Hara, T. Sato, R. Katoh, A. Furube, Y. Ohga, A. Shinpo, S. Suga, K. Sayama, H. Sugihara, H. Arakawa, J. Phys. Chem. B **107**, 597 (2003)
26. Z.-S. Wang, Y. Cui, Y. Dan-oh, C. Kasada, A. Shinpo, K. Hara, J. Phys. Chem. C **112**, 17011 (2008)
27. K. Hara, M. Kurashige, Y. Dan-oh, C. Kasada, A. Shinpo, S. Suga, K. Sayama, H. Arakawa, New J. Chem. **27**, 783 (2003)
28. K. Hara, Y. Tachibana, Y. Ohga, A. Shinpo, S. Suga, K. Sayama, H. Sugihara, H. Arakawa, Sol. Energy Mater. Sol. Cells **77**, 89 (2003)
29. A. Abbotto, L. Beverina, R. Bozio, S. Bradamante, C. Ferrante, G.A. Pagani, R. Signorini, Adv. Mater. **12**, 1963 (2000)
30. L.L. Estrella, S.H. Lee, D.H. Kim, Dyes Pigments **165**, 1 (2019)
31. Z.M.E. Fahim, S.M. Bouzzine, Y. Ait Aicha, M. Bouachrine, M. Hamidi, Res. Chem. Intermed. **44**, 2009 (2018)
32. B. Xu, E. Sheibani, P. Liu, J. Zhang, H. Tian, N. Vlachopoulos, G. Boschloo, L. Kloo, A. Hagfeldt, L. Sun, Adv. Mater. **26**, 6629 (2014)
33. N. Blouin, A. Michaud, M. Leclerc, Adv. Mater. **19**, 2295 (2007)
34. J. Li, F. Dierschke, J. Wu, A.C. Grimsdale, K. Müllen, J. Mater. Chem. **16**, 96 (2006)
35. Q. Li, L. Lu, C. Zhong, J. Shi, Q. Huang, X. Jin, T. Peng, J. Qin, Z. Li, J. Phys. Chem. B **113**, 14588 (2009)
36. D. Kim, M.-S. Kang, K. Song, S.O. Kang, J. Ko, Tetrahedron **64**, 10417 (2008)
37. T. Horiuchi, H. Miura, K. Sumioka, S. Uchida, J. Am. Chem. Soc. **126**, 12218 (2004)
38. S. Ito, H. Miura, S. Uchida, M. Takata, K. Sumioka, P. Liska, P. Comte, P. Péchy, and M. Grätzel, Chem. Commun. 5194 (2008).
39. D. Kuang, S. Uchida, R. Humphry-Baker, S.M. Zakeeruddin, M. Grätzel, Angew. Chem. Int. Ed. **47**, 1923 (2008)
40. A. Hagfeldt, G. Boschloo, L. Sun, L. Kloo, H. Pettersson, Chem. Rev. **110**, 6595 (2010)
41. K. Srinivas, K. Yesudas, K. Bhanuprakash, V.J. Rao, L. Giribabu, J. Phys. Chem. C **113**, 20117 (2009)
42. G. Wang, S. Miao, Q. Zhang, H. Liu, H. Li, N. Li, Q. Xu, J. Lu, L. Wang, Chem. Commun. **49**, 9470 (2013)
43. M. Guo, M. Li, Y. Dai, W. Shen, J. Peng, C. Zhu, S.H. Lin, R. He, RSC Adv. **3**, 17515 (2013)
44. L. Malak, H. Toufik, S.M. Bouzzine, H. Bih, F. Lamchouri **02**, 23 (2018)
45. Y.S. Yang, H.D. Kim, J.-H. Ryu, K.K. Kim, S.S. Park, K.-S. Ahn, J.H. Kim, Synth. Met. **161**, 850 (2011)
46. P. Shen, X. Liu, S. Jiang, L. Wang, L. Yi, D. Ye, B. Zhao, S. Tan, Dyes Pigments **92**, 1042 (2012)
47. W. Wu, J. Zhang, H. Yang, B. Jin, Y. Hu, J. Hua, C. Jing, Y. Long, H. Tian, J. Mater. Chem. **22**, 5382 (2012)
48. M. Lazrak, H. Toufik, S.M. Bouzzine, H. Bih, F. Lamchouri, I.O.P. Conf, Ser. Earth Environ. Sci. **161**, 012021 (2018)
49. S.P. Singh, M.S. Roy, A. Thomas, K. Bhanuprakash, G.D. Sharma, Org. Electron. **13**, 3108 (2012)
50. H. Jia, X. Ju, M. Zhang, Z. Ju, H. Zheng, Phys. Chem. Chem. Phys. **17**, 16334 (2015)
51. W. Lee, J. Choi, J.W. Namgoong, S.H. Kim, K.C. Sun, S.H. Jeong, K. Yoo, M.J. Ko, J.P. Kim, Dyes Pigments **104**, 185 (2014)
52. J. He, J. Hua, G. Hu, X.J. Yin, H. Gong, C. Li, Dyes Pigments **104**, 75 (2014)
53. J.T. Lin, P.-C. Chen, Y.-S. Yen, Y.-C. Hsu, H.-H. Chou, M.-C.P. Yeh, Org. Lett. **11**, 97 (2009)
54. K.D. Seo, I.T. Choi, H.K. Kim, Chem. Eur. J. **21**, 14804 (2015)
55. R. Li, X. Lv, D. Shi, D. Zhou, Y. Cheng, G. Zhang, P. Wang, J. Phys. Chem. C **113**, 7469 (2009)
56. A. Hagfeldt, M. Grätzel, Acc. Chem. Res. **33**, 269 (2000)
57. M.K. Nazeeruddin, A. Kay, I. Rodicio, R. Humphry-Baker, E. Mueller, P. Liska, N. Vlachopoulos, M. Graetzel, J. Am. Chem. Soc. **115**, 6382 (1993)
58. J. Preat, D. Jacquemin, E.A. Perpète, Environ. Sci. Technol. **44**, 5666 (2010)
59. R. Katoh, A. Furube, T. Yoshihara, K. Hara, G. Fujihashi, S. Takano, S. Murata, H. Arakawa, M. Tachiya, J. Phys. Chem. B **108**, 4818 (2004)

60. J.B. Asbury, Y.-Q. Wang, E. Hao, H.N. Ghosh, T. Lian, Res. Chem. Intermed. **27**, 393 (2001)
61. A. Mahmood, M. H. Tahir, A. Irfan, A. G. Al-Sehemi, and M. S. Al-Assiri, Comput. Theor. Chem. Complete, 94 (2015).
62. T. Marinado, K. Nonomura, J. Nissfolk, Martin. K. Karlsson, D. P. Hagberg, L. Sun, S. Mori, and A. Hagfeldt, Langmuir **26**, 2592 (2010).
63. S. Rühle, M. Greenshtein, S.-G. Chen, A. Merson, H. Pizem, C.S. Sukenik, D. Cahen, A. Zaban, J. Phys. Chem. B **109**, 18907 (2005)
64. W. Sang-aroon, S. Laopha, P. Chaiamornnugool, S. Tontapha, S. Saekow, V. Amornkitbamrung, J. Mol. Model. **19**, 1407 (2013)
65. Gaussian 09, Revision A.02, M. J. Frisch, G. W. Trucks, H. B. Schlegel, G. E. Scuseria, M. A. Robb, J. R. Cheeseman, G. Scalmani, V. Barone, G. A. Petersson, H. Nakatsuji, X. Li, M. Caricato, A. Marenich, J. Bloino, B. G. Janesko, R. Gomperts, B. Mennucci, H. P. Hratchian, J. V. Ortiz, A. F. Izmaylov, J. L. Sonnenberg, D. Williams-Young, F. Ding, F. Lipparini, F. Egidi, J. Goings, B. Peng, A. Petrone, T. Henderson, D. Ranasinghe, V. G. Zakrzewski, J. Gao, N. Rega, G. Zheng, W. Liang, M. Hada, M. Ehara, K. Toyota, R. Fukuda, J. Hasegawa, M. Ishida, T. Nakajima, Y. Honda, O. Kitao, H. Nakai, T. Vreven, K. Throssell, J. A. Montgomery, Jr., J. E. Peralta, F. Ogliaro, M. Bearpark, J. J. Heyd, E. Brothers, K. N. Kudin, V. N. Staroverov, T. Keith, R. Kobayashi, J. Normand, K. Raghavachari, A. Rendell, J. C. Burant, S. S. Iyengar, J. Tomasi, M. Cossi, J. M. Millam, M. Klene, C. Adamo, R. Cammi, J. W. Ochterski, R. L. Martin, K. Morokuma, O. Farkas, J. B. Foresman, and D. J. Fox, Gaussian, Inc., Wallingford CT (2016).
66. J. Preat, C. Michaux, D. Jacquemin, E.A. Perpète, J. Phys. Chem. C **113**, 16821 (2009)
67. Z. Fahim, S. M. Bouzzine, A. Youssef, M. Bouachrine, and M. Hamidi, Comput. Theor. Chem. **1125**, (2018).
68. R. Tarsang, V. Promarak, T. Sudyoadsuk, S. Namuangruk, S. Jungsuttiwong, J. Photochem. Photobiol. Chem. **273**, 8 (2014)
69. H. Toufik, S.M. Bouzzine, F. Lamchouri, M. Nawdali, M. Hamidi, M. Bouachrine, J. Mater. Environ. Sci. **3**, 286 (2012)
70. M. Lazrak, H. Toufik, S.M. Bouzzine, F. Lamchouri, Res. Chem. Intermed. **46**, 3961 (2020)
71. M. Grätzel, Nature **414**, 338 (2001)
72. S.U.-D. Khan, A. Mahmood, U.A. Rana, S. Haider, Theor. Chem. Acc. **134**, 1596 (2014)
73. S. Ennehary, H. Toufik, M. Lazrak, S.M. Bouzzine, F. Lamchouri, J. Mol. Model. **27**, 122 (2021)
74. M.A.M. Rashid, D. Hayati, K. Kwak, J. Hong, Nanomaterials **10**, 914 (2020)
75. G. Deogratias, O.S. Al-Qurashi, N. Wazzan, T. Pogrebnaya, A. Pogrebnoi, J. Mol. Model. **26**, 288 (2020)
76. S. Ennehary, H. Toufik, S.M. Bouzzine, F. Lamchouri, J. Comput. Electron. **19**, 840 (2020)
77. S. El Mzioui, S. M. Bouzzine, M. Bourass, M. Naciri Bennani, and M. Hamidi, J. Comput. Electron. **18**, 951 (2019).
78. M. Xie, J. Wang, F.-Q. Bai, L. Hao, H.-X. Zhang, Dyes Pigments **120**, 74 (2015)
79. M. Xie, F.-Q. Bai, J. Wang, C.-P. Kong, J. Chen, H.-X. Zhang, Comput. Mater. Sci. **111**, 239 (2016)
80. W. Zierkiewicz, M. Michalczyk, S. Scheiner, Molecules **23**, 1416 (2018)
81. S. Ito, S.M. Zakeeruddin, R. Humphry-Baker, P. Liska, R. Charvet, P. Comte, M.K. Nazeeruddin, P. Péchy, M. Takata, H. Miura, S. Uchida, M. Grätzel, Adv. Mater. **18**, 1202 (2006)
82. H. Kusama, K. Sayama, Phys. Chem. Chem. Phys. **17**, 4379 (2015)
83. H. Kusama, H. Sugihara, K. Sayama, J. Phys. Chem. C **115**, 2544 (2011)
84. Z. Liu, K. Duan, H. Guo, Y. Deng, H. Huang, X. Yi, H. Chen, S. Tan, Dyes Pigments **140**, 312 (2017)
85. H. Chen, Y. Gong, Á. Vázquez-Mayagoitia, J. Zhang, J.M. Cole, A.C.S. Appl, Energy Mater. **3**, 423 (2020)
86. J.K. Roy, S. Kar, J. Leszczynski, Sci. Rep. **8**, 10997 (2018)
87. R. Sánchez-de-Armas, M.A. San-Miguel, J. Oviedo, J. Fdez, Sanz. J. Chem. Phys. **136**, 194702 (2012)

Authors and Affiliations

Malak Lazrak[1] · Hamid Toufik[1] · Sliman Ennehary[1] · Si Mohamed Bouzzine[1,2] · Fatima Lamchouri[1]

[1] Laboratory of Natural Substances, Pharmacology, Environment, Modeling, Health and Quality of Life (SNAMOPEQ), Polydisciplinary Faculty of Taza, Sidi Mohamed Ben Abdellah University, Fez, Morocco

[2] Regional Center for Training and Professional Education, BP 8, Errachidia, Morocco